Materials & Design 82 (2015) 238–246

Contents lists available at ScienceDirect

Materials & Design

journal homepage: www.elsevier.com/locate/matdes

Shear coefficient determination in linear friction welding of aluminum alloys

Gianluca Buffa *, Marco Cammalleri, Davide Campanella, Livan Fratini

Department of Chemical, Management, Computer Science, Mechanical Engineering, University of Palermo, Italy

ARTICLE INFO

Article history:
Received 16 January 2015
Revised 4 May 2015
Accepted 30 May 2015

Keywords:
Linear friction welding
Shear coefficient
FEM model
Aluminum alloys

ABSTRACT

In the present study, a combined experimental and numerical investigation on Linear Friction Welding (LFW) of AA2011-T3 aluminum alloy was carried out in order to find the temperature dependent shear coefficient to be used in a 3D numerical model of the process. Torque, oscillation frequency and pressure were acquired in order to calculate the shear stress at the interface. A numerical thermal model was used to calculate the temperature at the interface between the specimens starting from experimental temperatures acquired through a thermocouple embedded in the LFW specimens. Finally, the calculated shear coefficient was used to model the contact between the two specimens in a dedicated 3D, Lagrangian, thermo-mechanically coupled rigid-viscoplastic numerical model of the LFW process. A narrow range of variation of the shear factor vs temperature curve was found with varying LFW process parameters and good agreement was obtained for the temperature prediction of the 3D model of the process.

1. Introduction

Linear Friction Welding (LFW) is a solid state welding process used to join bulk components. As a friction welding processes, solid bonding is obtained from the mechanical work decaying into heat in order to create a softened material which can be mixed and effectively joined. Different techniques can be used to create the needed frictional heat and consolidate the weld. Friction Stir Welding (FSW), the most recently introduced friction based welding process, is used to weld sheets in different configurations (butt, lap, T, etc.) [1–3]. A properly designed rotating tool is plunged between the adjoining edges of the sheets to be welded, producing the needed heat by friction forces work, while the stirring action of a pin induces the material flow. Rotary Friction Welding (RFW) and Inertia Friction Welding (IFW) [4] are used to join axisymmetric parts with particular reference to tubes. In the process, one tube is put into rotation and the other, inhibited from rotation, is forced against the former. No tool is needed.

In LFW, a reciprocation motion is generated between two bulk components and a forging pressure is applied in order to provide the needed heat input at the interface between the two parts to be welded [5,6]. Although the process was first patented by Walther Richter (Germany) in 1929 [7], no actual application or research activity was developed as the description of the motion was very vague and the process was labeled by Vill (Russia) in 1959 as "very doubtful". A considerable interest was shown by different industry sectors, but machines were considered too expensive. Reliable and lower cost machines were first developed in late 1990s. From that date, an increasing interest both in the academic and industrial fields was observed for LFW.

As the other solid bonding based techniques, LFW shows distinct advantages over traditional fusion welding processes, i.e. possibility to weld "unweldable" or difficult to be welded materials, absence of fumes, better material microstructure, joint integrity due to reduced grain size in the weld zone as well as lack of inclusions and porosities [8].

As far as LFW process mechanics [5] is regarded, the two materials are first brought in contact under pressure. At this stage, the two surfaces touch each other on asperities and the heat is generated from solid friction. Surface contact area is expected to increase throughout this phase with the reduction of asperities height. The heat input must be larger than the one lost by radiation or insufficient thermal softening occurs inhibiting the contact area to reach 100%. At this phase, instabilities can appear due to non-uniform temperature distribution at the interface or due to geometrical imperfections of the specimens. If sufficient heat is provided, the material is extruded from the four edges of the specimens and a reduction in height is observes. Finally, as the desired upset is reached, the reciprocating motion is stopped very quickly, i.e. in less than 0.1 s, and an increased forging pressure is simultaneously applied to consolidate the weld [9,10].

* Corresponding author.
E-mail address: gianluca.buffa@unipa.it (G. Buffa).

http://dx.doi.org/10.1016/j.matdes.2015.05.070
0264-1275/

Main process parameters are the pressure superimposed on the specimens to be welded, the frequency and the amplitude of oscillations of the specimens and the time length of the operation. These parameters must be properly determined for each base material to be welded in order to reach proper bonding conditions and to maximize the mechanical performances of the produced joints.

Several metal materials can be considered in the LFW process, namely steels [11,12], stainless steels [13], nickel based superalloys [14], titanium alloys [9,15], copper [16] and aluminum [17]. LFW of aluminum alloys can be very attractive for the possibility to weld with high efficiency aeronautical and aerospace aluminum alloys, namely AA2XXX and AA7XXX, in monolithic configurations. At the moment, very few applications of LFW of aluminum alloys are known. Rotundo et al. [18] demonstrated the feasibility of Dissimilar linear friction welding between a SiC particle reinforced aluminum MMC and AA2024, finding good tensile and fatigue properties, with respect to the AA2024 base material. In [19] the authors analyzed LFW joints obtained out of similar AA2024 specimens, finding joint efficiency of about 90%. In [20] Jun at al. obtained the residual strains in AA2024/AlSiCp linear friction welds, using a novel approach based on eigenstrain. Song et al. [21] studied the residual stress distribution in AA2024-T351 using both experiments and numerical simulation. Finally, Fratini et al. [17] studied LFW of AA6082-T6 aluminum alloy finding a process window depending on oscillation frequency and pressure. The lack of knowledge regarding LFW of aluminum alloys is also due to the difficulty in finding proper process parameters because of the material thermo-mechanical characteristics, namely thermal conductivity and heat capacity. The high thermal conductivity of these materials imposes that high heat must be input into the specimens in a reduced time, which is usually two to four time shorter than the one used for steel and titanium alloys. Consequently, large oscillation frequency values must be used to produce sound welds.

FEM can be an effective tool for the process design. As a matter of fact, due to the need to take into account, at the same time, technological, geometrical and metallurgical variables, the use of a numerical model can be very useful in the engineering of LFW of aluminum alloys. A reliable FEM model of the process can be used both to fully understand the process mechanics and to predict the actual bonding of the specimens through proper bonding criteria [22]. A few papers can be found in literature focusing on numerical simulation of LFW [23]. Most of the numerical models in literature, developed for titanium alloys, use a 2D approach with one of the two specimens modeled as a rigid-viscoelastic or elasto-plastic object and the other as a rigid one [24–26]. Li et al. [27] modeled the LFW of TC4 titanium alloy by a combination of explicit and implicit finite element analysis to study the influence of the main process parameters on axial shortening and temperature distribution. Song et al. [21] used a 2D approach with both specimens modeled as deformable objects to predict the residual stress in AA2024 LFW welds. A dedicated remeshing algorithm was used to take into account the large strain accumulated in the flash area. Recently, McAndrew et al. [28] used a novel approach, based on a single deformable body model [25]. The process is modeled starting by the onset of sticking friction, i.e. when the contact surface between the specimens is about 100% of the contact area and a viscous material flow is generated at the interface. Very good results can be obtained in terms flash morphology prediction and surface contaminant removal. However, an experimentally measured temperature field, taking into account the prior stages of the process, must be given to the model as initial condition. For most of the cited papers, a temperature depending shear coefficient was used to model the contact between the two specimens to be welded. It is worth noticing that this aspect is crucial in order to develop a reliable numerical model of the process. However, for none of the above cited papers details were provided on the determination of the shear coefficient curve.

In the paper, a combined experimental and numerical investigation is carried out on LFW of AA2011-T3, a high mechanical strength aluminum alloy used in the transportation industry for its excellent machinability, with the aim to determine the shear coefficient to be used in the numerical model of the process. It should be observed that this structural alloy is characterized by extremely poor weldability and thus welding is not recommended by traditional fusion welding techniques. In order to develop the experimental campaign, a previously in-house designed and built LFW machine was equipped with a number of measuring sensors [11,17]. Different tests were carried out with varying pressure and oscillation frequency. The data measured during the tests were collected and used to obtain the shear stress at the interface between the two specimens. Numerical results coming from both a pure thermal model and a thermos-mechanical model of the process were used to calculate the shear yield stress at the interface starting form experimental temperature measurements. Finally, the friction coefficient m as a function of process temperature at the interface was determined and validated using the 3D, thermo-mechanically coupled numerical model of the LFW process. In this way, an enhanced numerical model was obtained permitting to increase the accuracy and the quality of the acquired information.

2. Experimental approach

2.1. LFW machine

An in house developed experimental machine was used to carry out the experiments [17,29]. This machine uses a desmodromic kinematic chain in order to generate the oscillation motion of the bottom specimen. Two interchangeable cams with three lobes were chosen in order to widen the available range of oscillation frequency. The cams were assembled on two parallel shafts connected by coupling belt and pulleys [29]. An hydraulic actuator, fixed on a steel rack and controlled by an electro-valve, allowed to apply on the top specimen a pressure up to 250 MPa. A pneumatic clutch, activated by an electro-valve, and a micro-switch were used to control the start and finish of each experiment through a virtual instrument interface.

A number of devices and sensors, controlled by a unique interface, were introduced to increase the machine capabilities. A speed–torque meter was used on the secondary shaft to measure the required power and a fly wheel was adopted to balance the effects of inertia. A sketch of the main components of the machine is shown in Fig. 1.

A K-type thermocouple was fixed to the top specimen, at a distance of 6 mm from the specimens interface, to measure the temperature histories. All signals were conveyed to a National Instruments DAQ Card 6062 12 bit 500 kSa/s by means of a BNC-2120 connector and analyzed by a proper routine programmed with LabVIEW. The clutch was controlled by a pneumatic SMC solenoid valve and activated by the Labview interface. The clutch has the important function to obtain a quick stop reducing the machine inertia [20]. The software allowed to control the machine and monitor the process variables during and after the developed tests from a unique front panel.

2.2. Developed tests

The specimens, machined out of AA2011-T3 aluminum alloy bars, are characterized by height of 10 mm and cross-sectional dimensions at the contact interface equal to 10 mm × 7 mm.

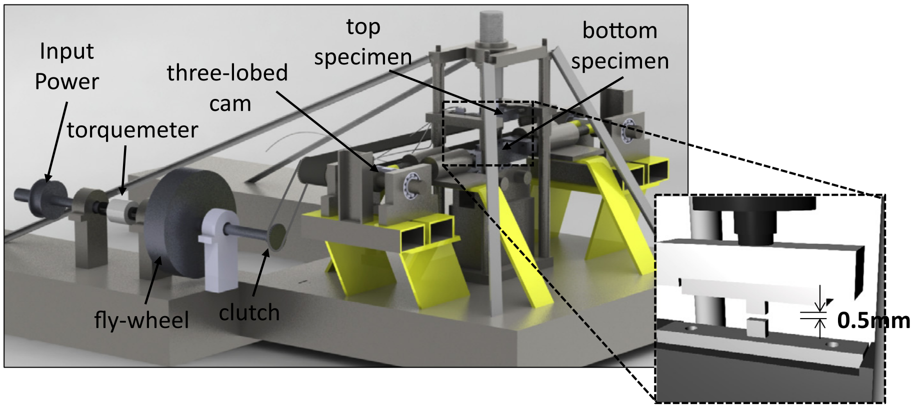

Fig. 1. Sketch of the machine with specimens in the starting position.

A hole, about 1 mm in diameter, was drilled on the lateral surface of the top specimen at a distance of 6 mm from the interface in order to fix a thermocouple for temperature acquisition during the process. Variable oscillation frequency and pressure were considered, while oscillation amplitude and process time were kept constant. The pneumatic clutch, controlled by the developed software interface, was released when the assigned process time ended thus instantly interrupting the reciprocating motion.

The process parameters used in this campaign are summarized in Fig. 2. These ranges of variation was chosen on the basis of previous study of the authors on aluminum alloys [CIRP] and a dedicated preliminary campaign on AA2011-T3. In particular, the six different combinations of oscillation frequency and interface pressure (dots in Fig. 2), resulting in sound joints, were used to acquire the data for the determination of the friction coefficient m. Two additional tests (cross in Fig. 2), outside the first domain, were used to validate the obtained friction coefficient by comparing experimentally measured and numerically calculated temperature. In particular, the 45 Hz–13 MPa case study corresponds to a "cold" joint due to the poor heat generated. On the contrary, the 71 Hz–40 MPa case study was a sound joint. Fixed oscillation amplitude, equal to 2 mm, and process time, equal to 1.5 s, were selected for all the tests. Each test was repeated three times and average curves were used for subsequent analysis. Good repeatability was obtained for all the tests with maximum variation of the acquired variable below 4%.

3. Numerical approach

3.1. Thermal model

A numerical model was used to calculate the temperature at the contact interface starting from an assigned heat flux conferred to the contact surface of the specimen. The commercial FEA software DEFORM-3D™, Lagrangian implicit code designed for metal forming processes, is used to model the thermal problem. Mechanical deformation was not taken into account in this model. As far as the thermal problem is regarded, the heat generation and transfer is expressed in the form of energy balance as follows,

$$K_1 T_{,ii} + \dot{r} - \rho c \dot{T} = 0 \quad (1)$$

where $k_1 T_{,ii}$ represents the heat transfer rate, $\dot{r}$ the heat generation rate and $\rho c \dot{T}$ the internal energy-rate.

The energy balance is written in the variation form

$$\int_V K_1 T_{,i} \delta T dV + \int_V \rho c \dot{T} \delta T dV - \int_V \alpha \sigma_{ij} \varepsilon_{ij} \delta T dV - \int_S q_n \delta T dS = 0 \quad (2)$$

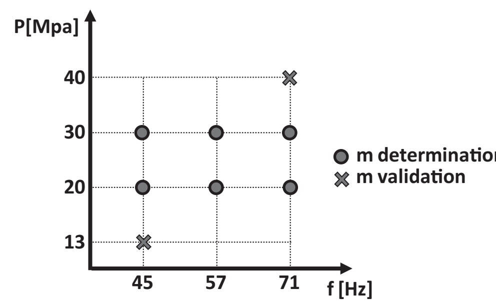

Fig. 2. Pressure and oscillation frequency used for the determination of the friction coefficient and the validation of the results.

where α is the fraction of mechanical work decaying into heat. Hence, this is not considered in this model but it will be taken into account for the model of the LFW process as described in the following sub-paragraph. q_n is the heat flux across the boundary surface S,

$$q_n = k_q T_{,n} \quad (3)$$

To solve problems of this nature, it is required that the temperature field satisfies the prescribed boundary conditions and Eq. (3) for arbitrary perturbation δT. The finite element formulation for temperature analysis can be expressed as

$$[C]\{\dot{T}\} + [K_c]\{T\} = \{Q\} \quad (4)$$

Temperature is often found by the finite difference approximation

$$T_{t+\Delta t} = T_t + \Delta t[(1-\beta)\dot{T}_t + \beta \dot{T}_{t+\Delta t}] \quad (5)$$

The convergence of Eq. (5) depends on the choice of the parameter β. It is usually considered that β should be larger than 0.5 to ensure an unconditional stability and a value of 0.75 is commonly selected.

The experimental specimen was meshed, for thermal analysis only, with about 10,000 tetrahedral elements. An external heat flux was assigned as boundary condition to the contact surface of the specimen. The value of the heat flux is a function of the combination of interface pressure and oscillation frequency utilized. Hence, a different value was utilized for each case study. The methodology used to calculate the heat flux will be described in the following paragraph. Fig. 3 shows a close up of the meshed specimen used for the thermal model.

The following constant values were used for the thermal properties of the considered AA2011-T3 aluminum alloy: thermal conductivity 180.2 N/s K, heat capacity 2.433 N/mm^2 K. Preliminary

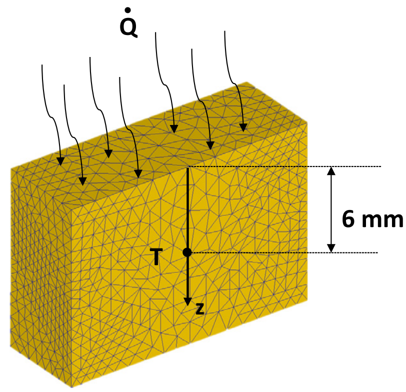

Fig. 3. Close up of the specimen meshed for the thermal analysis.

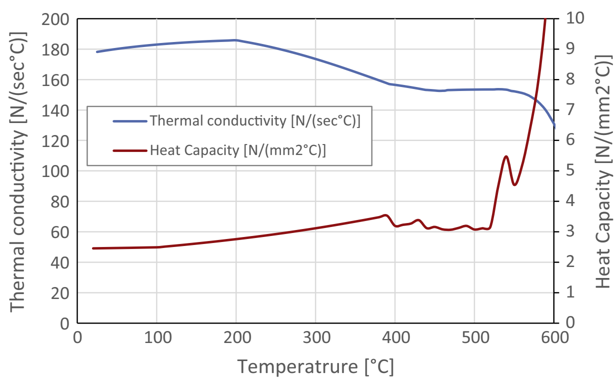

Fig. 4. Thermal conductivity and heat capacity vs. temperature used for the preliminary analyses.

simulations were run using temperature dependent heat capacity and thermal conductivity. The data were taken from the Jmatpro material database. Fig. 4 shows the used curves.

The thermal analysis was carried out using both temperature dependent and constant thermal data. The result of these simulations is shown in Fig. 5.

Very similar thermal profiles are calculated, although a slightly colder specimen is predicted using the temperature dependent data. This is due to the combined effect of increasing heat capacity and decreasing thermal conductivity with temperature, with respect to the reference values used (2.43 and 180, respectively). The observed limited impact on the temperature distribution is due to the relatively small variations of heat capacity and thermal conductivity in the temperature ranges occurring during the considered process, i.e. about 20–400 °C, and to the limited process time. Additionally, this assumption, used also for the thermo-mechanical model, linearizes the thermal Eq. (4) and results in better convergence.

3.2. Thermo-mechanical model

The simulation campaign was carried out using a thermo-mechanically coupled 3D model set up with DEFORM 3D™. The rigid-viscoplastic finite element formulation is based on the variational approach. According this approach, the actual velocities (i.e. the actual solution) among all admissible velocities u_i that satisfy the conditions of compatibility and incompressibility, as well as the velocity boundary conditions, gives the following functional a stationary value

$$\pi = \int_V E(\dot{\varepsilon}_{ij})dV - \int_{S_v} F_i u_i dS \tag{6}$$

where E denotes the work function. The incompressibility constraint on admissible velocity fields is removed by introducing a penalized form of the incompressibility in the variation of the functional. Therefore, the actual velocity field is determined from the stationary value of the variation as follows,

$$\delta\pi = \int_V \bar{\sigma}\delta\dot{\bar{\varepsilon}}dV + k\int_V \dot{\varepsilon}\delta\dot{\varepsilon}dV - \int_{S_F} F_i\delta u_i dS_F = 0 \tag{7}$$

It is worth noticing that the penalty constant K should be very large positive constant for incompressibility.

The LFW process was simulated by modeling the top specimen as a deformable object having the same geometry of the experimental specimens. The bottom specimen was modeled as a rigid plate, meshed for thermal analysis only. Although this approach is less accurate than modeling both the specimens as rigid-visco-plastic objects, it is widely used in literature [24–26] due to its simplicity and significantly faster convergence, making it suitable for industrial applications. Due to the geometrical symmetry of the process, a symmetry plane was placed along the oscillating direction in order to simulate half of each object, reducing the computational cost in 3D. Each simulated sample has 10 × 3.5 × 7 mm dimensions and was meshed using tetrahedral element with mesh density decreasing with the distance from

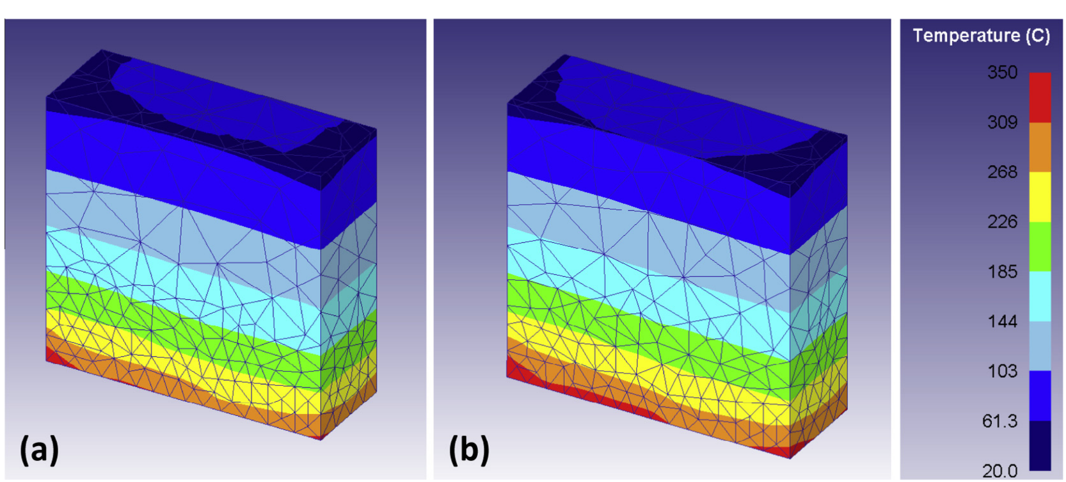

Fig. 5. Thermal profiles obtained with (a) variable thermal data and (b) constant thermal data.

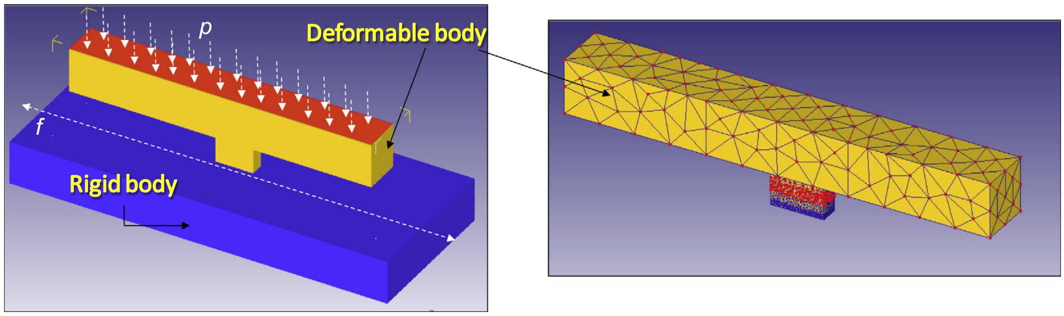

Fig. 6. Assembled model highlighting the surface used for the pressure boundary condition and the constrained nodes.

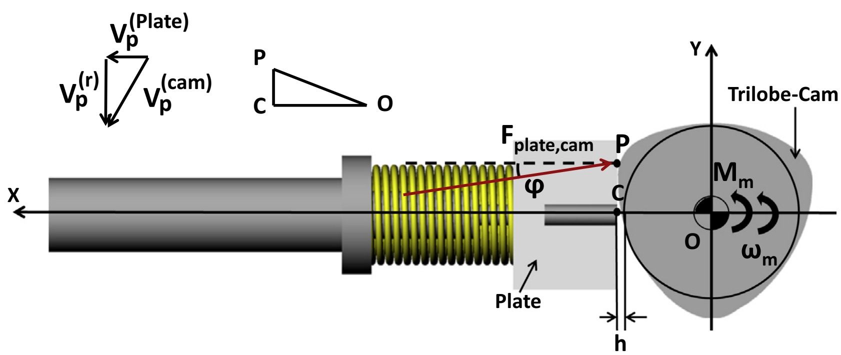

Fig. 7. Sketch of the contact between the cam and the plate highlighting forces and velocity.

the contact interface, thus optimizing the calculation time. The mesh of the most distant area from the contact interface includes elements having size of about 1.2 mm, the middle zone is meshed using elements with a fixed size of 0.3 mm, while the contact zone is meshed using elements with a fixed size of 0.15 mm. This mesh set-up resulted in about 32,000 elements per sample. A fixed time-step of 0.0001 s was used in all simulations. The choice of this small value, although resulting in increased CPU time, was driven form the need to correctly follow the fast movement of the oscillating specimen. The heat transfer coefficient with external air was 0.02 N/(s mm °C). Due to the LFW process mechanics, the thermal exchange coefficient at the contact interface typically used for forging processes was used. In particular, a heat exchange coefficient of 11 N(s mm °C) was selected. Every analysis started at room temperature. The contact conditions were modeled using the shear model. A friction coefficient function of temperature was determined through the used combined experimental and numerical approach. An initial constant value of m equal to 0.7 was used for the iterative procedure described in the next paragraph. The final friction coefficient expression was used for the validation of the approach proposed in this paper.

The visco-plastic behavior of the AA2011-T3 aluminum alloy was modeled by a temperature and strain rate dependent flow stress curves based on both literature data and previous preliminary numerical campaign [29,30]. The oscillation was assigned to the rigid plate while an external pressure was assigned, as a boundary condition, to the top deformable specimen in order to have at the interface the desired contact pressure. The nodes of the top specimen far from the contact interface were constrained against movement in the X and Y directions. Fig. 6 shows the assembled model as well as the mesh of the top specimen and the constrained nodes (red[1] dots in Fig. 6).

[1] For interpretation of color in Fig. 6, the reader is referred to the web version of this article.

4. Shear coefficient determination

It is known that the shear coefficient is the ratio between the shear stress acting on the contact surface and the material shear yield stress.

$$m = \frac{\tau(p, f, t)}{\tau_0(p, f, t)} \tag{8}$$

Being p the interface pressure, f the oscillation frequency and t the process time. For each case study, both the shear stress, which is generated by the simultaneous action of the reciprocating motion and the applied normal pressure, and the shear yield stress vary with time. The shear yield stress is a function of temperature and strain rate, which vary during the process until the reciprocation motion is stopped. Temperature and strain rate, in turn, depends on the main process parameters, namely oscillation frequency, pressure and time. In the following sub-paragraphs, the procedures used to calculate the shear stress and the shear yield stress at the contact interface are described.

4.1. Tangential stress

Fig. 7 shows, for a generic configuration, a sketch of the contact between the cam and the plate highlighting forces and velocity.

The three-lobes cam profile was designed to impose an harmonic movement to the specimen, so

$$\begin{aligned} h &= A[1 - \cos(3\vartheta)] \\ h' &= 3A\sin(3\vartheta) \\ h'' &= 9A\cos(3\vartheta) \\ \ddot{h} &= \omega_m^2 h''(\vartheta) \end{aligned} \tag{9}$$

where A is the amplitude of oscillation, i.e. the half-stroke of the plate. Note that the velocity triangle and OPC triangle are similar, so that:

$$\frac{\mathrm{PC}}{\mathrm{OP}} = \frac{V_p^{(plate)}}{V_p^{(cam)}} \Rightarrow \mathrm{PC} = \frac{dh}{d\vartheta} = h' \tag{10}$$

OC = $r_b + h$, where r_b is the cam base radius and h stands for the plate displacement from the right dead center. Combining the cam rotational and the plate horizontal equilibrium conditions with the above equations it can be written:

$$M_m = (F_w + M\ddot{h})[h' + (r_b + h)f] \tag{11}$$

where $f = \tan\varphi$ is the Coulomb friction coefficient between the cam and the plate, M indicates the overall oscillating mass, and F_w represents the welding force, that is the shear force acting on the contact surface between the top and the bottom specimen. At this stage, only the losses in the cam-plate contact are taken into account. Thus, the instantaneous inlet power, P_m, into the LFW machine is:

$$\begin{aligned} P_m &= [P_w] + [P_f] \\ &= [(F_w + m\ddot{h})h'\omega_m] + [(F_w + m\ddot{h})(r_b + h)fh'\omega_m] \end{aligned} \tag{12}$$

where P_w is the welding power and P_f the lost friction power. It should be noticed that, for the development of the thermal model described in Section 3.1, it was considered that $P_w = \dot{Q}$. In this way, it was assumed that both the friction forces work and the entire deformation work decay into heat. This assumption can be considered reasonable for most metals, for which the energy lost for microstructural change is negligible with respect to the two above cited energies. $P_T = M_T\omega_T$ is the power measured by speed-torque meter (see Fig. 1) and P_L is the power lost in the mechanical system, except for in the cam-plate contact, the power balance imposes

$$P_T = P_w + P_f + P_L \tag{13}$$

Named M_{T_0} the measured torque in unloaded conditions, that is when $F_w = 0$, after some algebra and averaging on one stroke, the expression of the average welding force $\overline{F_w}$ as a function of the experimentally measured torques results:

$$\overline{F_w} = \frac{\overline{M_T} - \overline{M_{T_0}}}{R\left[\frac{6A}{\pi} + f(r_b + A)\right]} \tag{14}$$

where $R = \frac{\omega_m}{\omega_T}$ denotes the rigid speed ratio between cam shaft and measurement shaft.

Named $\overline{S} = ab\left(1 - \frac{a}{b}\frac{2}{\pi}\right)$, being $a = 10$ mm and $b = 7$ mm, the average contact area between the welding specimens the shear stress τ is:

$$\tau = \frac{\overline{F_w}}{\overline{S}} \tag{15}$$

Fig. 8 shows the off-load and in-process torque together with the burn off, i.e. the shortening of the specimens along the direction normal to the contact surface, experimentally measured during the LFW tests for the 57 Hz–30 MPa case study.

The shear stress τ and the heat flux $\dot{Q}$, used for the thermal model, obtained for the same case study considered in Fig. 8, are shown in Fig. 9.

4.2. Shear yield stress

As already mentioned, the shear yield stress is a function of temperature and strain rate. Due to the nature of the process, it is extremely difficult to measure the temperature at the interface between the specimens. In turn, temperature can be easily measured through a thermocouple in one of the specimens. The thermal model described in Section 3.1 was used to calculate the temperature evolution with time for 60 reference points laying on the symmetry plane (i.e. where the thermocouple measures temperature during the experiments) and equally spaced by 0.1 mm. The reference points were placed along the z axis (see again Fig. 3), ranging from $z = 0$ mm, namely the contact interface, to $z = 6$ mm, namely the position of the thermocouple at the beginning of the process. Fig. 10 shows the variation of temperature with the distance from the contact interface at different times for the 57 Hz–30 MPa case study. For sake of simplicity only the lower curve, corresponding to $t = 0$ s, and the higher curve, corresponding to the end of the process ($t = 1.5$ s), are labeled.

It is worth noticing that the distance between the thermocouple and the contact interface decreases during the welding due to the burn off. A temperature multiplier λ was built according to the following expression:

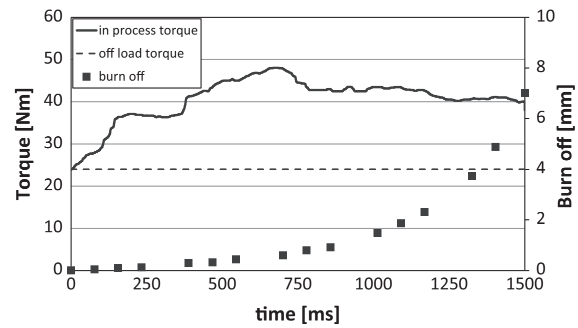

Fig. 8. Burn off, off-load and in-process torque measured for the 57 Hz–30 MPa case study.

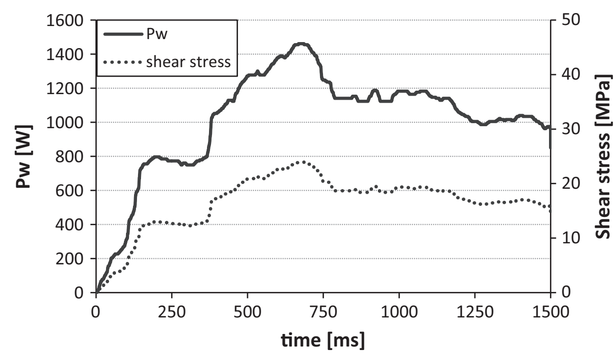

Fig. 9. Shear stress and heat flux used for the thermal model for the 57 Hz–30 MPa case study.

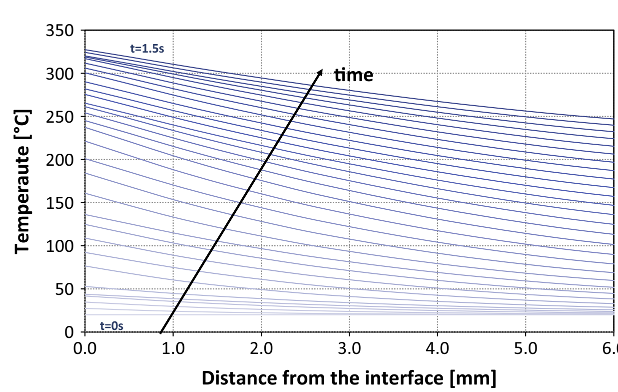

Fig. 10. Temperature vs distance from the contact interface at different times as calculated by the thermal model for the 57 Hz–30 MPa case study.

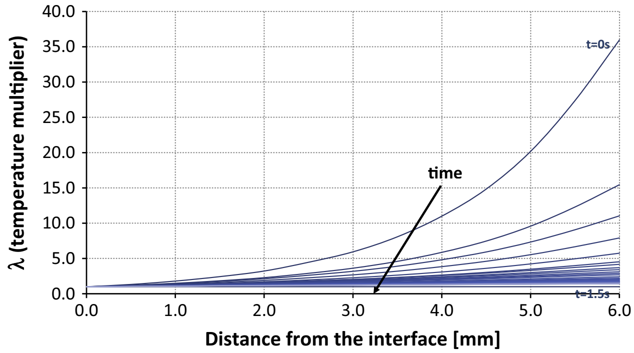

Fig. 11. Temperature multiplier λ at different times as calculated by the thermal model for the 57 Hz–30 MPa case study.

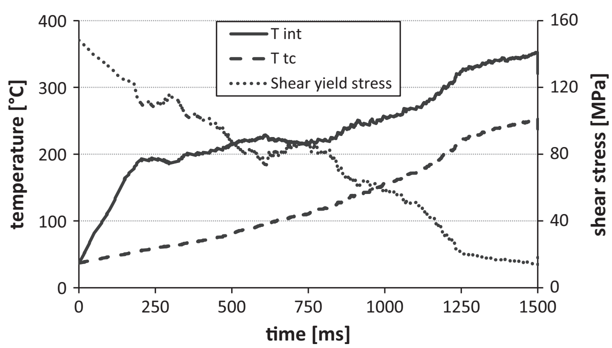

Fig. 12. Acquired temperature T_{tc}, calculated temperature T_{int} and shear yield stress for the 57 Hz–30 MPa case study.

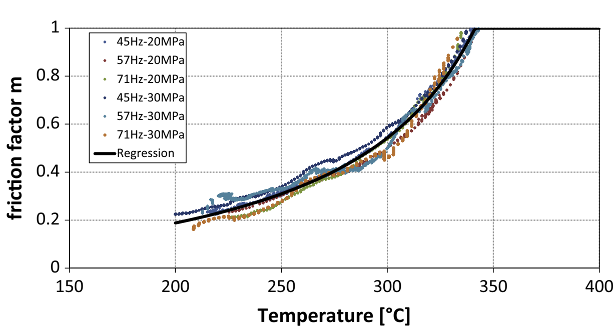

Fig. 13. Friction coefficient m vs. temperature for the six considered case studies and average curve obtained by regression.

$$\lambda = \frac{T_{int} - T_0}{T_{tc} - T_0} \tag{16}$$

where T_{int} is the temperature at the interface, T_0 is the room temperature and T_{tc} is the temperature measured by the thermocouple. In Fig. 11 the λ values obtained for the same case study considered in Fig. 11 are plotted. Again, just the curves corresponding to $t = 0$ s and $t = 1.5$ s are labeled. It is worth noticing that, due to the nature of the thermal problem (Section 2.1), the λ values are the same for each case study, i.e. for each value imposed as boundary condition.

In order to estimate the strain rate an iterative procedure was followed. A constant value of the friction coefficient m equal to 0.7 was used to simulate, through the thermo-mechanical model of the process, each case study. The strain rate evolution with time at the interface was collected and used to determine the shear yield stress. Then, the resulting m function (see next paragraph for further details) was utilized as input for a new set of simulations of the six case studies. This loop was repeated until the difference between the strain rate obtained in two consecutive runs was below 5% for all the case studies. In this way, for any time ranging from $t = 0$ s and $t = 1.5$ s, using the experimental burn off to calculate the actual distance between the thermocouple and the interface, it was possible to calculate the temperature at the interface and, finally, the shear yield stress τ_0.

The temperature T_{tc} acquired through the thermocouple, the temperature T_{int} calculated by the temperature multiplier λ and the obtained shear yield stress τ_0 are shown for the 57 Hz–30 MPa case study in Fig. 12.

5. LFW model validation

The procedure described in the previous paragraph permitted to calculate the friction coefficient m, as a function of temperature, for each of the considered case studies (Fig. 13). The six curves obtained showed good consistency and a regression was carried out to find an average m function to be used in the numerical model of the process. A constant value of 0.2 was assigned to the friction coefficient for $T < 200$ °C, which is the friction coefficient for cold aluminum–aluminum contact. The calculated curve reaches a value equal to 1 at $T = 340$ °C. Hence, the m value was considered constant for temperature values in excess of this threshold. The following equation was thus obtained:

$$m = \begin{cases} 0.2 & T < 200\,^\circ\mathrm{C} \\ \frac{-0.196T}{T-408} & 200\,^\circ\mathrm{C} < T < 340\,^\circ\mathrm{C} \\ 1 & T > 340\,^\circ\mathrm{C} \end{cases} \tag{17}$$

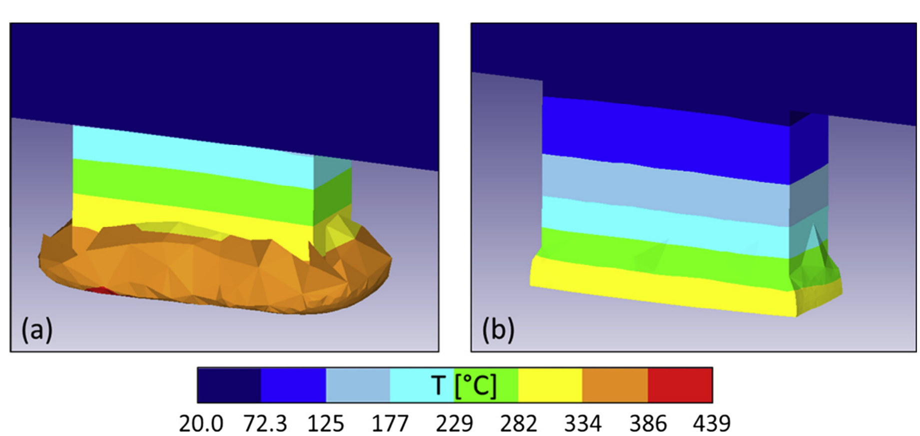

Fig. 14. 3D temperature profiles of the specimens area close to the contact surface for the (a) 71 Hz–40 MPa and (b) 45 Hz–13 MPa case studies.

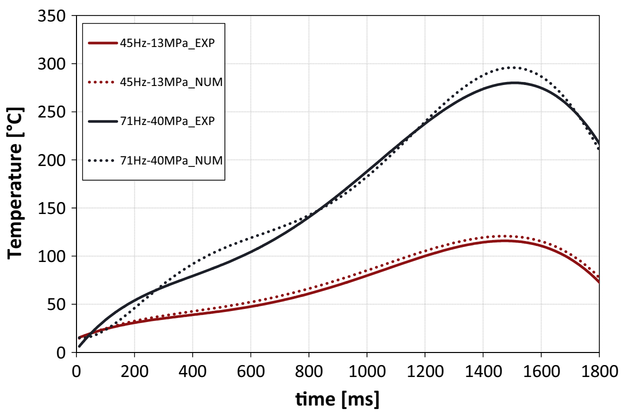

Fig. 15. Experimental vs numerical temperature history in the thermocouple position for the 71 Hz–40 MPa and 45 Hz–13 MPa case studies.

It is worth noticing that the relative simplicity of the expression found for the shear friction coefficient contributes to keep the CPU time needed for the simulation of the process as short as possible. The obtained friction coefficient was finally used for the thermo-mechanical simulation of the process. Two case studies were considered, namely the 45 Hz–13 MPa and the 71 Hz–40 MPa (see again Fig. 2). It should be observed that the former combination of process parameters results in an ineffective joint due to the low heat input. On the contrary, a sound joint was obtained with $f = 71$ Hz and $p = 40$ MPa. Fig. 14 shows a close up of the 3D temperature profiles obtained for the two case studies.

The temperature history numerically calculated in a reference point placed at an initial distance from the interface equal to 6 mm, corresponding to the position of the thermocouple, was compared to the experimentally measured one (Fig. 15). It is worth noticing that a lagrangian approach was followed for the definition of the reference point. In other words, the point moves according to the material flow following the position of the experimental thermocouple.

A good agreement was found, especially for the 45 Hz–13 MPa case study, as far as both the trend and the maximum values are regarded. For the 71 Hz–40 MPa case study, the model overestimates the maximum experimental temperature by about 15 °C, corresponding to about +5%.

6. Summary and conclusions

In the paper, the results from a combined experimental and numerical investigation, aimed to the identification of the temperature dependent friction coefficient to be used in a dedicated numerical model of the LFW process, are presented. Aluminum alloy AA2011-T3 was taken into account.

Different values of interface pressure and oscillation frequency were used to define the six case studies used for the determination of the friction coefficient.

Torque, temperature and burn off were experimentally measured during the tests. Additionally, both a thermal model, used to study the heat diffusion in the specimens, and a thermo-mechanical model of the LFW process were developed.

The shear stress acting on the contact interface was calculated starting from the experimental measurements of off-load and in-process torque and burn off. The shear yield stress was calculated by an integrated experimental/numerical approach starting from the temperature measurements and using both the thermal and the thermo-mechanical model.

A simple analytical expression, function of temperature, was found for the friction coefficient and used to simulate two further processes out of the process window considered for the determination of the friction coefficient. In particular, the process parameters resulting in a sound joint and a poor joint were selected for the result validation. Good agreement was obtained for both the tests between the temperature numerically calculated and experimentally measured by the thermocouple thus enhancing the numerical model and making it suitable for future analysis of process mechanics and bonding mechanisms during the LFW process.

References

[1] R.S. Mishra, Z.Y. Ma, Friction stir welding and processing, Mater. Sci. Eng. 50 (2005) 1–78.
[2] L. Fratini, G. Buffa, F. Micari, R. Shivpuri, On the material flow in FSW of T-joints: influence of geometrical and technological parameters, Int. J. Adv. Manuf. Technol. 44 (2009) 570–578.
[3] G. Buffa, G. Campanile, L. Fratini, A. Prisco, Friction stir welding of lap joints: influence of process parameters on the metallurgical and mechanical properties, Mater. Sci. Eng., A 519 (2009) 19–26.
[4] H.-S. Jeong, J.-R. Cho, J.-S. Oh, E.-N. Kim, S.-G. Choi, M.-Y. Ha, Inertia friction welding process analysis and mechanical properties evaluation of large rotor shaft in marine turbo charger, Int. J. Precis. Eng. Manuf. 11 (2010) 83–88.
[5] A. Vairis, M. Frost, High frequency linear friction welding of a titanium alloy, Wear 217 (1998) 117–131.
[6] A. Vairis, M. Frost, On the extrusion stage of linear friction welding of Ti 6a1 4V, Mater. Sci. Eng., A 271 (1999) 477–484.
[7] Herbeifuehrung einer Haftverbindung zwischen Plaettchen aus Werkzeugstahl und deren Traegern nach Art einer Schweissung oder Loetung Herbeifuehrung a bond between Flakes made of tool steel and their carriers on the type of welding or soldering. Google Patents, 1929.
[8] I. Bhamji, M. Preuss, P.L. Threadgill, A.C. Addison, Solid state joining of metals by linear friction welding: a literature review, Mater. Sci. Technol. 27 (2011) 2–12.
[9] E. Dalgaard, P. Wanjara, J. Gholipour, X.b. Cao, J.J. Jonas, Linear friction welding of a near-β titanium alloy, Acta Mater. 60 (2012) 770–780.
[10] J. Romero, M.M. Attallah, M. Preuss, M. Karadge, S.E. Bray, Effect of the forging pressure on the microstructure and residual stress development in Ti–6Al–4V linear friction welds, Acta Mater. 57 (2009) 5582–5592.
[11] L. Fratini, G.L. Buffa, D. La Spisa, Effect of process parameters in linear friction welding processes of steels, in: Proceedings of the 10th International Conference on Technology of Plasticity, ICTP 2011, 2011, pp. 746–751.
[12] L. Fratini, G. Buffa, D. Campanella, D. La Spisa, Investigations on the linear friction welding process through numerical simulations and experiments, Mater. Des. 40 (2012) 285–291.
[13] I. Bhamji, M. Preuss, P.L. Threadgill, R.J. Moat, A.C. Addison, M.J. Peel, Linear friction welding of AISI 316L stainless steel, Mater. Sci. Eng., A 528 (2010) 680–690.
[14] O.T. Ola, O.A. Ojo, P. Wanjara, M.C. Chaturvedi, Analysis of microstructural changes induced by linear friction welding in a nickel-base superalloy, Metall. Mater. Trans. A 42 (2011) 3761–3777.
[15] C.-C. Zhang, J.-H. Huang, T.-C. Zhang, Y.-J. Ji, The analysis in linear friction welding joint interface behavior of dissimilar titanium alloy, Cailiao Gongcheng/J. Mater. Eng. (2011) 80–84.
[16] E. Dalgaard, P. Wanjara, G. Trigo, M. Jahazi, G. Comeau, J.J. Jonas, Linear friction welding of Al–Cu part 2 – interfacial characteristics, Can. Metall. Q. 50 (2011) 360–370.
[17] L. Fratini, G. Buffa, M. Cammalleri, D. Campanella, On the linear friction welding process of aluminum alloys: experimental insights through process monitoring, CIRP Ann. – Manuf. Technol. 62 (2013) 295–298.
[18] F. Rotundo, A. Marconi, A. Morri, A. Ceschini, Dissimilar linear friction welding between a SiC particle reinforced aluminum composite and a monolithic aluminum alloy: microstructural, tensile and fatigue properties, Mater. Sci. Eng., A 559 (2013) 852–860.
[19] F. Rotundo, A. Morri, L. Ceschini, Linear friction welding of a 2024 Al alloy: microstructural, tensile and fatigue properties, TMS Light Met. (2012) 493–496.
[20] T.S. Jun, F. Rotundo, X. Song, L. Ceschini, A.M. Korsunsky, Residual strains in AA2024/AlSiCp composite linear friction welds, Mater. Des. 31 (2010) S117–S120.
[21] X. Song, M. Xie, F. Hofmann, T.S. Jun, T. Connolley, C. Reinhard, R.C. Atwood, L. Connor, M. Drakopoulos, S. Harding, A.M. Korsunsky, Residual stresses in Linear Friction Welding of aluminium alloys, Mater. Des. 50 (2013) 360–369.
[22] G. Buffa, G. Patrinostro, L. Fratini, Using a neural network for qualitative and quantitative predictions of weld integrity in solid bonding dominated processes, Comput. Struct. 135 (2014) 1–9.
[23] A. Vairis, M. Frost, Modelling the linear friction welding of titanium blocks, Mater. Sci. Eng., A 292 (2000) 8–17.
[24] S.K. Kiselyeva, A.M. Yamileva, M.V. Karavaeva, I.S. Nasibullayev, V.M. Bychkov, A.Y. Medvedev, A.V. Supov, F.F. Musin, I.V. Alexandrov, V.V. Latysh, Computer modelling of linear friction welding based on the joint microstructure, J. Eng. Sci. Technol. Rev. 5 (2012) 44–47.
[25] R. Turner, J.-C. Gebelin, R.M. Ward, R.C. Reed, Linear friction welding of Ti–6Al–4V: modelling and validation, Acta Mater. 59 (2011) 3792–3803.

[26] A.M. Yamileva, A.V. Yuldashev, I.S. Nasibullayev I.Sh., Comparison of the parallelization efficiency of a thermo-structural problem simulated in SIMULIA Abaqus and ANSYS mechanical, J. Eng. Sci. Technol. Rev. 5 (2012) 39–43.
[27] W.Y. Li, T. Ma, J. Li, Numerical simulation of linear friction welding of titanium alloy: effects of processing parameters, Mater. Des. 31 (2010) 1497–1507.
[28] A.R. McAndrew, P.A. Colegrove, A.C. Addison, B.C.D. Flipo, M.J. Russell, Modelling the influence of the process inputs on the removal of surface contaminants from Ti–6Al–4V linear friction welds, Mater. Des. 66 (2015) 183–195.
[29] D.C. Gianluca Buffa, Antonello D'annibale, Di Ilio Antoniomaria, Livan Fratini, Experimental and numerical study on linear friction welding of AA2011 aluminum alloy, Key Eng. Mater. 611–612 (2014) 1511–1518.
[30] ASM Specialty Handbook: Aluminum and Aluminum Alloys: ASM International, 1993.